7164 *Biochemistry* **2010,** *49,* 7164–7178
DOI: 10.1021/bi100930u

BIOCHEMISTRY
including biophysical chemistry & molecular biology
Article

Thermotoga maritima Ribonuclease III. Characterization of Thermostable Biochemical Behavior and Analysis of Conserved Base Pairs That Function as Reactivity Epitopes for the *Thermotoga* 23S rRNA Precursor[†]

Lilian Nathania[‡] and Allen W. Nicholson*[,‡,§]

[‡]*Departments of Chemistry and* [§]*Biology, Temple University, Philadelphia, Pennsylvania 19122*

Received June 9, 2010; Revised Manuscript Received July 17, 2010

ABSTRACT: The cleavage of double-stranded (ds) RNA by ribonuclease III is a conserved early step in bacterial rRNA maturation. Studies on the mechanism of dsRNA cleavage by RNase III have focused mainly on the enzymes from mesophiles such as *Escherichia coli*. In contrast, neither the catalytic properties of extremophile RNases III nor the structures and reactivities of their cognate substrates have been described. The biochemical behavior of RNase III of the hyperthermophilic bacterium *Thermotoga maritima* was analyzed using purified recombinant enzyme. *T. maritima* (Tm) RNase III catalytic activity exhibits a broad optimal temperature range of ~40−70 °C, with significant activity at 95 °C. Tm-RNase III cleavage of substrate is optimally supported by Mg^{2+} at ≥1 mM concentrations. Mn^{2+}, Co^{2+}, and Ni^{2+} also support activity but with reduced efficiencies. The enzyme functions optimally at pH 8 and ~50−80 mM salt concentrations. Small RNA hairpins that incorporate the 16S and 23S pre-rRNA stem sequences are efficiently cleaved by Tm-RNase III at sites that are consistent with production *in vivo* of the immediate precursors to the mature rRNAs. Analysis of pre-23S substrate variants reveals a dependence of reactivity on the base-pair (bp) sequence in the proximal box (pb), a site of protein contact that functions as a positive recognition determinant for *Escherichia coli* (Ec) RNase III substrates. The dependence of reactivity on the pb sequence is similar to that observed with Ec-RNase III substrates. In fact, Tm-RNase III cleaves an Ec-RNase III substrate with identical specificity and is inhibited by antideterminant bp that also inhibit Ec-RNase III. These results indicate the conservation, across a broad phylogenetic distance, of positive and negative determinants of reactivity of bacterial RNase III substrates.

The maturation and degradation of bacterial RNAs involve the coordinated action of endoribonucleases, 3′→5′ exoribonucleases, and 5′→3′ exoribonucleases (reviewed in refs *1* and *2*). The current understanding of bacterial RNA processing and decay pathways is based primarily on studies using a relatively limited set of mesophiles that includes *Escherichia coli* and *Bacillus subtilis*. In contrast, comparatively little is known of the RNA processing pathways and associated ribonucleases of bacterial extremophiles. Ongoing biochemical and structural studies of proteins of the hyperthermophilic bacterium *Thermotoga maritima* (*3*−*6*) are providing essential insight on the origins of biomolecular thermostability (*7*, *8*). The *T. maritima* (Tm)[1] genome encodes a relatively limited set of ribonucleases (*3*, *9*), several of which have been characterized. Tm-RNase P has been purified and shown to accurately cleave pre-tRNA substrates *in vitro*, and the protein subunit can confer thermostability on the *E. coli* RNA subunit *in vitro* (*10*). Structural studies reveal that the protein subunit is dimeric (*11*) and that the RNA subunit exhibits conserved domains and specific RNA−RNA interactions important for substrate binding and cleavage (*12*). Structural and biochemical studies of Tm-tRNase Z (RNase Z) have (i) established a dimeric protein structure with a metallo-β-lactamase fold (*13*), (ii) identified specific residues essential for phosphodiesterase activity (*14*), and (iii) established a novel pathway for tRNA 3′-end formation involving cleavage at a site directly downstream of the encoded CCA sequence (*15*).

Ribonuclease III is a double strand-specific endonuclease that is highly conserved in bacteria and participates in diverse RNA maturation and decay pathways (reviewed in refs (*16*−*22*)). RNase III controls antibiotic production in the *Streptomyces* (*23*−*26*), regulates virulence factor expression in *Staphylococcus* (*27*), participates in bacteriophage strategies of infection (*28*, *29*), and functions in antisense RNA-mediated gene regulation (*30*, *31*). RNase III has a conserved role in bacterial rRNA maturation that involves the site-specific cleavage of double-helical structures associated with the termini of the 16S and 23S rRNAs (*32*−*34*). The RNase III catalytic mechanism involves activation of water that cleaves each strand at a double-helical target site, affording products with 5′-phosphate, 3′-hydroxyl termini. RNase III requires a divalent metal ion for activity, and structural (*35*, *36*), kinetic (*37*), and inhibitor (*37*) studies support a two-metal-ion catalytic mechanism. Bacterial RNase III polypeptides are ~220 amino acids in length and exhibit an N-terminal domain containing conserved carboxylic acid residues essential for catalytic activity and a C-terminal dsRNA-binding domain (dsRBD) containing a single copy of the conserved dsRNA-binding motif (dsRBM) (Figure 1B). The bacterial RNase III holoenzyme is formed by dimerization of the nuclease domain and therefore contains two functionally independent catalytic sites and two dsRBDs, with both copies of the latter domain required for optimal catalytic activity *in vitro* (*38*, *39*). A recently characterized RNase III

[†]This work was supported by NIH Grant GM56772.
*Corresponding author. Telephone: (215) 204-9048. Fax: (215) 204-1532. E-mail: anichol@temple.edu.
[1]Abbreviations: db, distal box; dsRNA, double-stranded RNA; pb, proximal box; RBM, RNA-binding motif; RNase, ribonuclease; Ec, *Escherichia coli*; Tm, *Thermotoga maritima*.

 Published on Web 07/22/2010 © 2010 American Chemical Society

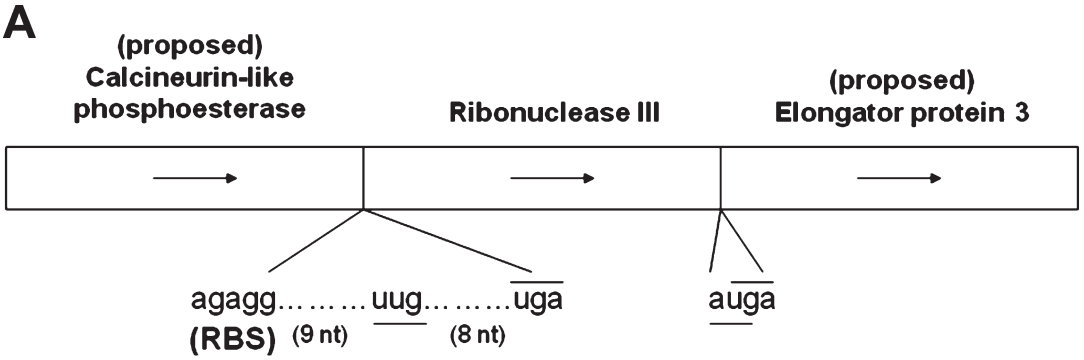

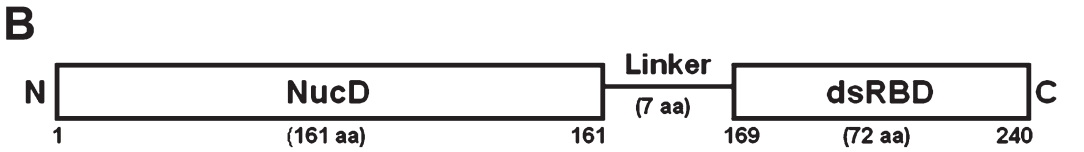

C

```
                                                                    RBM 4
T. maritima       MNESERKIVE EFQKETGINF KNEELLFRAL CHSSYANEQN QAGRKD VES NEKLEFLGDA  59
A. aeolicus       -----MKMLE QLEKKLGYTF KDKSLLEKAL THVSYS---- ------KKEH YETLEFLGDA  45
M. tuberculosis   ----MIRSRQ PLLDALGVDL -PDELLSLAL THRSYAYENG ------GLPT NERLEFLGDA  49
E. coli           ---MNPIVIN RLQRKLGYTF NHQELLQQAL THRSAS---- ------SK-H NERLEFLGDS  46

                                                                    RBM 4
T. maritima       VLELFVCEIL YKKYPEAEVG DLARVKSAAA SEEVLAMVSR KM---NLGKF LFLGKGEEKT  116
A. aeolicus       LVNFFIVDLL VQYSPNKREG FLSPLKAYLI SEEFFNLLAQ KL---ELHKF IRIKRG--KI  100
M. tuberculosis   VLGLTITDAL FHRHPDRSEG DLAKLRASVV NTQALADVAR RLCAEGLGVH VLLGRGEANT  109
E. coli           ILSYVIANAL YHRFPRVDEG DMSRMRATLV RGNTLAELAR EF---ELGEC LRLGPGELKS  103

                                                          Flexible Linker
T. maritima       GGRDRDSILA DAFEALLAAI YLDQ--GYEK IKELFEQEFE FYIEKIMK-G EMLFD        168
A. aeolicus       ----NETIIG DVFEALWAAV YIDSGRDANF TRELFYKLFK EDILSAIKEG RVKKD        157
M. tuberculosis   GGADKSSILA DGMESLLGAI YLQH--GMEK AREVILRLFG PLLDAAPTLG AGL-D        155
E. coli           GGFRRESILA DTVEALIGGV FLDS--DIQT VEKLILNWYQ TRLDEI-SPG DKQKD        161

                  RBM 1
T. maritima       YKTALQEIVQ SEHKVPPEYI LVRTEKNDGD RIFVVEVRVN GKTIAT-GKG RTKKEAEKEA  227
A. aeolicus       YKTILQEITQ KRWKERPEYR LISVEGPHHK KKFIVEAKIK -EYRTL-GEG KSKKEAEQRA  209
M. tuberculosis   WKTSLQELTA ARGLGAPSYL VTSTGPDHDK EFTAVVVVMD SEYGS--GVG RSKKEAEQKA  213
E. coli           PKTRLQEYLQ GRHLPLPTYL VVQVRGEAHD QEFTIHCQVS GLSEPVVGTG SSRRKAEQAA  215


T. maritima       ARIAYEKLLK ERS-------- 240
A. aeolicus       AEELIKLLEE SE--------- 221
M. tuberculosis   AAAAWKALEV LDNAMPGKTSA 234
E. coli           AEQALKKLEL E---------- 226
```

FIGURE 1: *T. maritima* RNase III gene and protein features. (A) The *T. maritima* RNase III gene and its genetic neighborhood. Arrows indicate the proposed directions of transcription. The noncanonical UUG translation initiation codon for Tm-RNase III is indicated and is 8 nt upstream of the UGA stop codon of the open reading frame (ORF) for the proposed calcineurin-like phosphoesterase gene. The putative ribosome binding site (RBS) is 9 nt upstream of the start codon. The proposed UGA stop codon for Tm-RNase III overlaps the AUG start codon for the ORF of the proposed elongator protein 3. A potential promoter (not shown) is present within the proposed calcineurin-like phosphoesterase gene, and a potential terminator (not shown) is downstream of the proposed elongator protein 3 gene, suggesting coupled transcription and translation of the RNase III and elongator protein 3 genes. (B) Domain structure of the Tm-RNase III polypeptide. The N-terminal nuclease domain (NucD) encompasses 161 amino acids and is connected by a 7-residue linker to the C-terminal dsRNA-binding domain (dsRBD) (72 amino acids). (C) Comparison of Tm-RNase III amino acid sequence with those of *A. aeolicus*, *M. tuberculosis*, and *E. coli*. Shown are the positions of the NucD, linker, dsRBD, RBM1, and RBM4.

family member ("Mini-III") from *B. subtilis* lacks the dsRBD and participates in 23S rRNA maturation with the assistance of ribosomal protein L3 (*40*, *41*).

Essential insight on the RNase III mechanism of action has been provided by structural analyses of the *Aquifex aeolicus* enzyme, which was crystallized in the presence of various divalent metal ions or with short dsRNAs or RNA hairpins (*35*, *42*−*45*). These studies revealed the symmetric positioning of the two catalytic sites across the subunit interface and demonstrated the positional mobility of the dsRBD. A crystallographic study of *Mycobacterium tuberculosis* RNase III also revealed dsRBD mobility and identified an additional binding site for divalent metal ion (Ca^{2+}) that is close to the two catalytic metal sites (*46*). A crystallographic study of Dicer from *Giardia intestinalis* revealed an essentially identical arrangement of catalytic sites in the nuclease domain that possesses an intramolecular pseudo-dimeric structure and the conservation of carboxylic acid residues involved in binding the catalytic metals (*36*).

A 2.0 Å structure of *T. maritima* (Tm) RNase III was reported by the Joint Center for Structural Genomics (PDB entry 1O0w),

which reveals, among other features, the two dsRBDs in extended symmetric positions with respect to the nuclease domain. This structure, along with the *A. aeolicus* RNase III structures, provided the basis for a proposed pathway of dsRNA recognition and cleavage by bacterial RNases III (*35*). However, the biochemical properties of Tm-RNase III have not been reported, and a characterization of the structures and reactivities of cognate substrates is lacking. This information would provide the basis for the functional description, referenced to a known structure, of the elementary steps in the RNase III mechanism of dsRNA processing and also could assess the possible conservation of reactivity epitopes of bacterial RNase III substrates. We present here a study of the biochemical properties of purified recombinant Tm-RNase III and an analysis of sequence-dependent processing reactivities of small RNA hairpins based on the *Thermotoga* 16S and 23S pre-rRNAs.

EXPERIMENTAL PROCEDURES

Materials. Water was deionized and distilled. Chemicals and reagents were of molecular biology grade and were purchased either from Sigma-Aldrich or Fisher Scientific. Standardized 1 M solutions of $MgCl_2$ and $MnCl_2$ were obtained from Sigma-Aldrich. Ribonucleoside 5′-triphosphates were obtained from Roche Molecular Biochemicals. [γ-^{32}P]ATP (3000 Ci/mmol), [α-^{32}P]UTP (3000 Ci/mmol), and [5′-^{32}P]pCp (3000 Ci/mmol) were purchased from Perkin-Elmer. *E. coli* bulk stripped tRNA was purchased from Sigma-Aldrich and was further purified by repeated phenol extraction followed by ethanol precipitation. The gene for Tm-RNase III (Figure 1A) was amplified from a sample of *T. maritima* DNA (a generous gift of Francis Jenney, University of Georgia) and cloned into plasmid pET-15b (Novagen) as described (*47*). Production of recombinant Tm-RNase III used the *E. coli* expression strain, BL21(DE3)*rnc*105*rec*A, that carries an inactivating mutation (*rnc105*) of the chromosomal RNase III gene (*48*). Cell cultures were grown at 37 °C, and protein expression was induced by IPTG addition as described (*47*, *48*). The protein was purified from the soluble portion of sonicated cell extracts (previously clarified by centrifugation) using Ni^{2+} affinity chromatography (*47*, *48*). *E. coli* RNase III was purified as described previously (*47*). The experiments presented in this study used Tm-RNase III that retained the $(His)_6$ tag.

RNA Synthesis. Oligodeoxynucleotides used as transcription templates were synthesized by Invitrogen and provided in deprotected form. The DNAs were purified by denaturing polyacrylamide gel electrophoresis and stored at −20 °C in 10 mM Tris-HCl and 1 mM EDTA (pH 8) (*48*). Bacteriophage T7 RNA polymerase was purified as described (*49*). Internally ^{32}P-labeled RNAs were synthesized and purified by gel electrophoresis as described (*48*, *50*, *51*). The specific activity of the UTP in the transcription reactions (100 μL volume) was 150 Ci/mol. RNA was 5′-^{32}P-labeled using T4 polynucleotide kinase (New England Biolabs) and [γ-^{32}P]ATP, followed by gel electrophoretic purification (*48*). Prior to labeling, the RNA was treated with shrimp alkaline phosphatase (Roche Biochemicals). Alternatively, RNA was ^{32}P-labeled at the 3′-end using [5′-^{32}P]pCp (3000 Ci/mmol) and T4 RNA ligase (New England Biolabs) as described (*52*) and purified by gel electrophoresis.

RNA Cleavage Assay. Substrate cleavage assays were performed using purified Tm-RNase III and ^{32}P-labeled RNA. Prior to use, RNA was heated in TE buffer at 100 °C for 30 s and then placed on ice. The standard assay was performed at 45 °C in a buffer consisting of 50 mM NaCl, 1 mM $MgCl_2$, and 30 mM Tris-HCl (pH 8) (see also Results). Either divalent metal ion or RNA was added to initiate the reaction, as specified in the relevant figure legends. Additional assay conditions, including Tm-RNase III and RNA concentrations, are also provided in the relevant figure legends. Reactions were stopped by adding an equal volume of a gel loading/stop solution containing 20 mM EDTA, 7 M urea, 30% glycerol (v/v), and bromophenol blue (0.04%) in TBE buffer (*48*). Aliquots were analyzed by electrophoresis in 15% polyacrylamide gels containing 7 M urea and TBE buffer. Reactions were visualized by phosphorimaging (Typhoon 9400 system) and analyzed by ImageQuant software.

Gel Mobility Shift Assay. Gel mobility shift assays were performed using 5′-^{32}P-labeled RNA essentially as described (*48*). To dissociate any intermolecular RNA complexes formed upon storage at −20 °C, ^{32}P-labeled RNA (10^4 cpm) was heated in TE buffer (pH 8) at 100 °C for 1 min and then placed on ice. The binding reaction buffer consisted of 250 mM potassium glutamate, 30 mM Tris-HCl (pH 8.0), 5 mM NaCl, 5 mM spermidine, 1 mM DTT, 1 mM EDTA, and 5% (v/v) glycerol. Five millimolar $CaCl_2$ was included in the reaction and electrophoresis buffers. The reaction mixture was incubated at 37 °C for 10 min and then placed on ice for 20 min, tRNA (500 ng/μL final concentration) was then added to the reaction, and aliquots were directly loaded onto an 8% polyacrylamide gel (80:1 acrylamide:*N*,*N*′-methylenebisacrylamide) containing 0.5× TBE buffer and 5 mM $CaCl_2$. Electrophoresis was performed at ∼5−6 °C at 100 V. Binding reactions were visualized by phosphorimaging, and the nonequilibrium dissociation constants (K'_D values) were determined using ImageQuant software as described (ref *53*; see Supporting Information Figure 2).

RESULTS

Divalent Metal Ion Dependence of Tm-RNase III Catalytic Activity. We examined different divalent metal ions for their ability to support Tm-RNase III catalytic activity. The substrate used was Tm-23S[hp] RNA, a small RNA hairpin that is based on the *Thermotoga* pre-23S rRNA processing stem. This RNA is characterized in more detail below. Tm-RNase III cleavage of internally ^{32}P-labeled Tm-23S[hp] RNA was measured as a function of metal ion concentration, with short reaction times applied to limit the extent of cleavage. Figure 2A shows that Mg^{2+} supports cleavage of the RNA, with maximal activity achieved at ∼1 mM Mg^{2+}. Mn^{2+} also supports substrate cleavage, with an optimal concentration of ∼2 mM, but with a lower maximal activity compared to Mg^{2+} (Figure 2B). Co^{2+} supports activity with an apparent optimal concentration of ∼0.5 mM but also inhibits cleavage at higher concentrations (Figure 2B). Ni^{2+} supports only negligible levels of activity (Figure 2B), and Ca^{2+} is inactive over the range of examined concentrations (data not shown). Based on these results, Mg^{2+} (1 mM) was incorporated in the standard cleavage assay buffer.

Salt and pH Dependence of Tm-RNase III Catalytic Activity. The dependence of Tm-RNase III catalytic activity on salt type and concentration was assessed using internally ^{32}P-labeled Tm-23S[hp] RNA. The salt (Na^+, K^+, or NH_4^+, with Cl^- as anion) concentration ranged between 30 and 330 mM. Cleavage assay results are graphically summarized in Figure 3A, where it is seen that Tm-RNase III is most active within the ∼50−80 mM concentration range for each cation. Tm-RNase III exhibits a modest preference in the order $NH_4^+ > K^+ > Na^+$

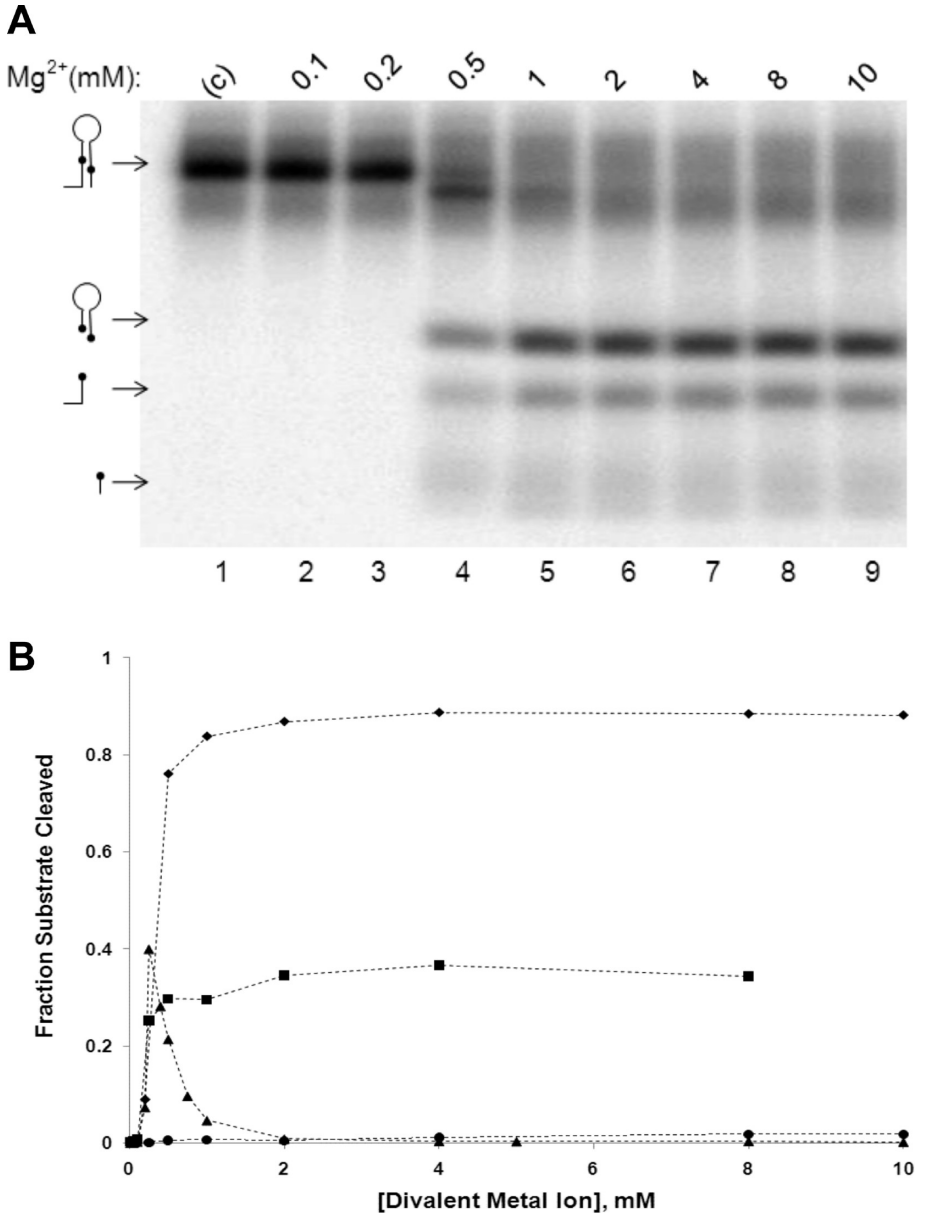

FIGURE 2: Divalent metal ion dependence of Tm-RNase III catalytic activity. (A) Mg^{2+} dependence of Tm-RNase III catalytic activity. The assay used internally ^{32}P-labeled Tm-23S[hp] RNA (see Figure 5C) (10^4 dpm) and Tm-RNase III (25 nM). The reaction buffer contained Mg^{2+} (as the chloride salt) at the concentrations given at the top of the image and also contained 50 mM NaCl and 30 mM Tris-HCl (pH 8.0). Reactions were initiated by addition of RNA, incubated at 45 °C for 1 min, and then stopped by addition of gel loading solution containing 20 mM EDTA (see Experimental Procedures). Aliquots were electrophoresed in a 15% polyacrylamide gel containing 7 M urea in TBE buffer. The fraction of substrate cleaved was determined by ImageQuant analysis. The control experiment (C) in lane 1 consisted of incubating RNA and protein in the absence of Mg^{2+}. The figures on the left of the image indicate the positions of the substrate and the three cleavage products. The additional cleavage product seen in lane 4, which is directly underneath the substrate, is probably a product of cleavage of one of the two scissile phosphodiesters. (B) Graphic display of dependence of Tm-RNase III catalytic activity on the type and concentration of divalent metal ion. Points represent the average of duplicate assays. Key: diamonds, Mg^{2+}; squares, Mn^{2+}; triangles, Co^{2+}; circles, Ni^{2+}.

(Figure 3A). The pH dependence of Tm-RNase III activity was determined using Tm-23S[hp] RNA as substrate and employing HEPES buffer with the pH ranging between 6.4 and 9.0. The results (Figure 3B) reveal that optimal catalytic activity is attained at a pH ~8, with the shape of the curve in the transition region suggesting the involvement one or more ionizable groups with an apparent pK_a of ~7.5 and with the conjugate base form exhibiting greater activity. Based on these results, the standard reaction buffer included NaCl at 50 mM and a pH of 8, with Na^+ chosen to avoid NH_4^+ ion volatility or potential interfering K^+−RNA interactions.

Thermostability of Tm-RNase III Catalytic Activity. The temperature dependence of Tm-RNase III catalytic activity was assessed and compared with that of *E. coli* (Ec) RNase III. Tm-23S[hp] RNA was used in both assays to avoid differential effects of temperature on substrate structure. The Mg^{2+} and Na^+ concentrations were 1 and 50 mM, respectively, and HEPES buffer (pH 8) was employed in order to minimize temperature-dependent pH changes. Reactions that were otherwise complete except for substrate were brought to the specified temperature, and RNA was added to initiate the reaction, followed by incubation for 1 min. Reactions were quenched with excess EDTA and aliquots analyzed by gel electrophoresis. Panels A and B of Figure 4 show representative cleavage assays using Tm-RNase III and Ec-RNase III, respectively. Figure 4C displays the fraction of substrate cleaved by each enzyme as a function of

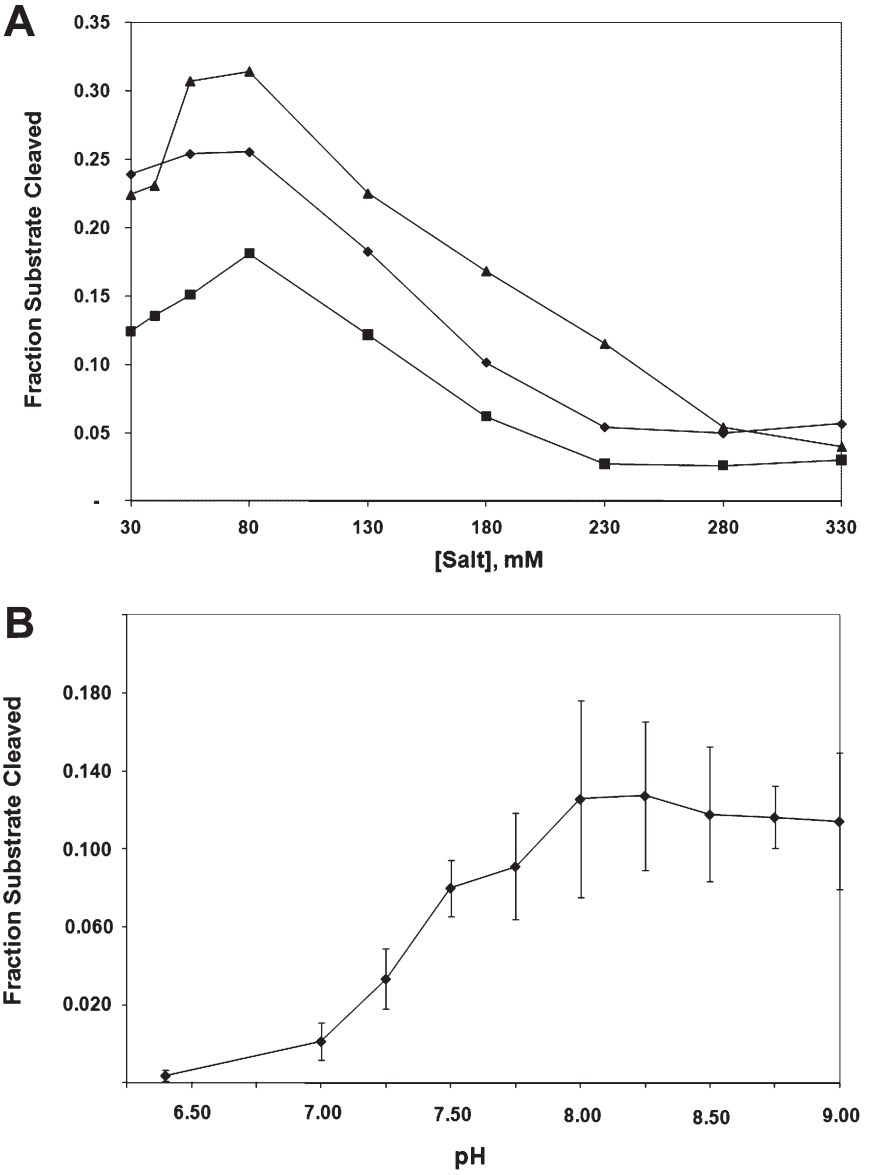

FIGURE 3: Salt and pH dependence of Tm-RNase III catalytic activity. (A) Monovalent cation type and concentration dependencies. Cleavage reactions involved 128 nM (10^4 dpm) internally ^{32}P-labeled Tm-23S[hp] RNA (Figure 5C), 25 nM Tm-RNase III, 1 mM $MgCl_2$, and 30 mM Tris-HCl, pH 8. The chloride salts of Na^+ (triangles), K^+ (diamonds), and NH_4^+ (squares) were examined at the specified concentrations. The initial salt concentration (NaCl) that accompanied the enzyme was 30 mM in the three experiments. Reactions were performed and analyzed as described above and in Experimental Procedures. (B) pH dependence. Cleavage assays involved internally ^{32}P-labeled Tm-23S[hp] RNA (10^4 dpm, 128 nM) and 25 nM Tm-RNase III. The reaction buffer contained 50 mM NaCl, 1 mM $MgCl_2$, and 30 mM HEPES adjusted to the specified pH values between 6.4 and 9.0. Reactions were performed at 45 °C for 1 min and analyzed as described above. The points represent the average of two experiments, with the maximum error indicated by the bars.

temperature. The results show that Tm-RNase III catalytic activity exhibits a broad optimum of ~40−70 °C and is sustained up to ~95 °C, albeit at a lower level (Figure 4A,C). In contrast, Ec-RNase III catalytic activity exhibits a lower temperature range of ~20−50 °C, with essentially no activity observed above ~55 °C (Figure 4B,C). We conclude that Tm-RNase III exhibits substantial thermostability, and based on these results an experimentally convenient temperature of 45 °C was used as a standard assay condition.

Site-Specific Cleavage of RNA Hairpins Based on the Thermotoga 16S and 23S rRNA Processing Stems. The *T. maritima* chromosome contains a single locus that encodes the three rRNAs in the standard order of 16S-23S-5S and also encodes three tRNAs (Figure 5A) (*3*). While the promoter and terminator have not been identified, transcription of this locus would produce an ~5000 nt RNA in which the 16S and 23S rRNA sequences are topologically demarked by pairing of the 5′ and 3′ flanking sequences (Figure 5A). Such base-paired stem structures are conserved in the bacteria (*32*) and have been shown in other species to be targets of site-specific cleavage by RNase III as an initial step in the maturation pathway (*33*, *34*). Panels B and C of Figure 5 show the sequences and proposed secondary structures of the Tm 16S and 23S processing stems. The two stems are similar in length (~32 and ~28 bp of uninterrupted base pairs, respectively) and exhibit central regions of high sequence similarity. Two RNA hairpins, Tm-16S[hp] RNA and Tm-23S[hp] RNA (panels B and C of Figure 5, respectively), were prepared that incorporated the central portions of the respective processing stems. A time course for cleavage of each RNA in internally ^{32}P-labeled form is shown in Figures 6A,B (Tm-RNase III cleavage of Tm-23S[hp] RNA as a function of Mg^{2+} concentration is shown in Figure 2A). Both Tm-16S[hp] RNA

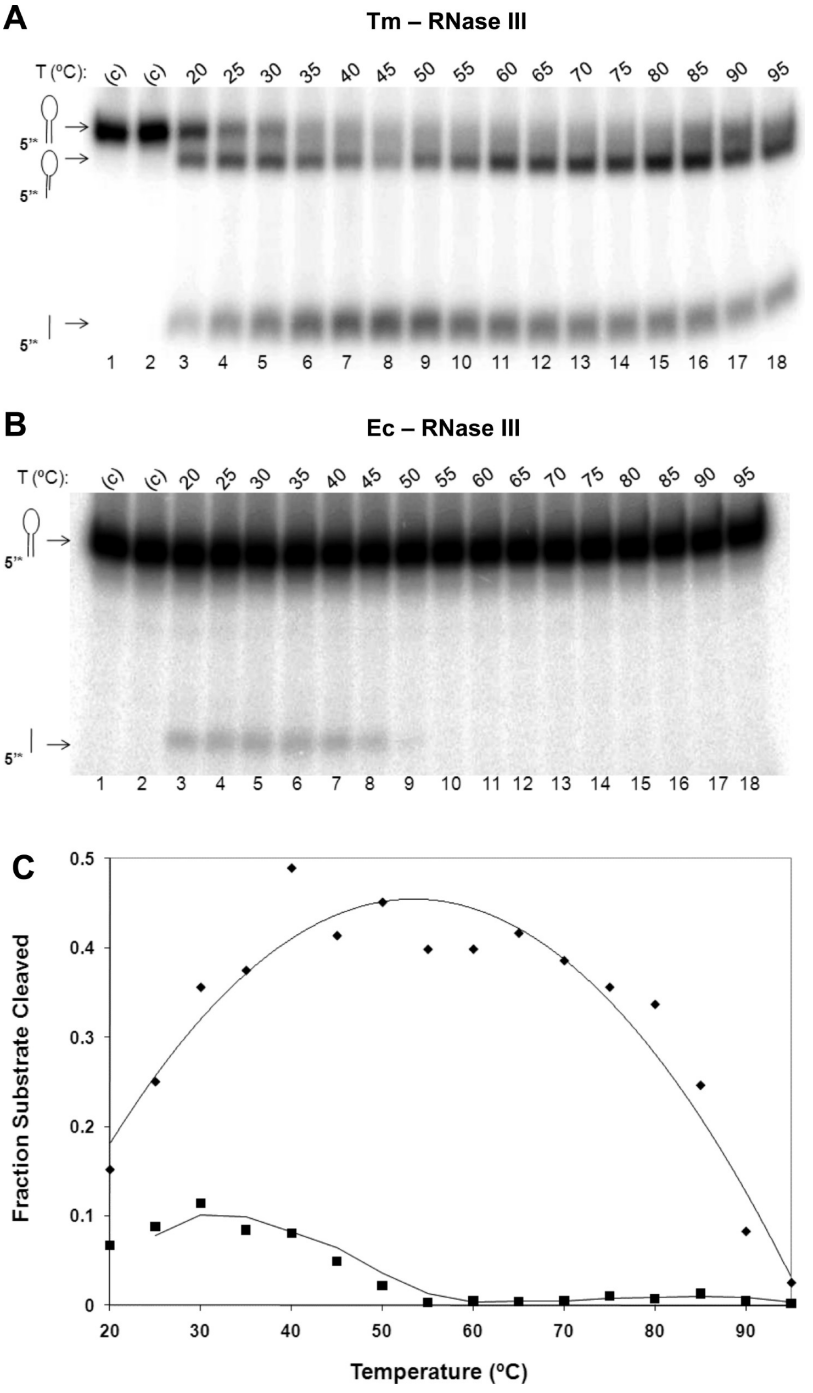

FIGURE 4: Thermostable catalytic activity of Tm-RNase III. (A) Tm-RNase III cleavage of Tm-23S[hp] RNA as a function of temperature. Reactions included 5′-^{32}P-labeled Tm-23S[hp] RNA (77 pM, 5×10^3 dpm) and Tm-RNase III (25 nM) in a buffer consisting of 50 mM NaCl, 1 mM $MgCl_2$, and 30 mM HEPES (pH 8.0). Prior to use, RNA was heated in TE buffer at 100 °C for 1 min and then placed on ice. The enzyme was incubated at the specified temperature for 1 min in reaction buffer containing Mg^{2+}, and the reaction was started by addition of RNA. Reactions were incubated for 1 min and then quenched by excess EDTA, and aliquots were electrophoresed in a 15% polyacrylamide gel containing 7 M urea in TBE buffer (see also Experimental Procedures). The fraction of substrate cleaved was determined by phosphorimaging and ImageQuant analysis. The positions of the substrate and the two 5′-^{32}P-labeled products of cleavage are indicated on the left side of the phosphorimage. (B) Ec-RNase III cleavage of 5′-^{32}P-labeled Tm-23S[hp] RNA as a function of temperature. Reactions were performed as described above, except that Ec-RNase III (25 nM) was substituted for Tm-RNase III. The positions of the substrate and the 5′-end-containing cleavage product are shown on the left of the phosphorimage. Compared to the Tm-RNase III experiment in (A), there was no product that resulted from cleavage of the phosphodiester on the target site 3′-side. (C) Graphic comparison of Tm-RNase III and Ec-RNase III catalytic activity as a function of temperature, as measured by fraction of substrate cleaved. Points represent the average of two experiments. Key: diamonds, Tm-RNase III; squares, Ec-RNase III.

and Tm-23S[hp] RNA are cleaved to form three specific products, indicating the selective hydrolysis of two phosphodiesters within each RNA. The 3′-end-containing cleavage products exhibit size heterogeneity (Figure 6A,B), which most likely reflects the nontemplated addition of one or two additional nucleotides by T7 RNA polymerase during transcription, as has been noted elsewhere (*50*, *51*). The cleavage sites were mapped by comparing the gel electrophoretic mobilities of the products of Tm-RNase III cleavage of 5′-^{32}P-labeled or 3′-^{32}P-labeled Tm-16S[hp] RNA and Tm-23S[hp] RNA with the corresponding

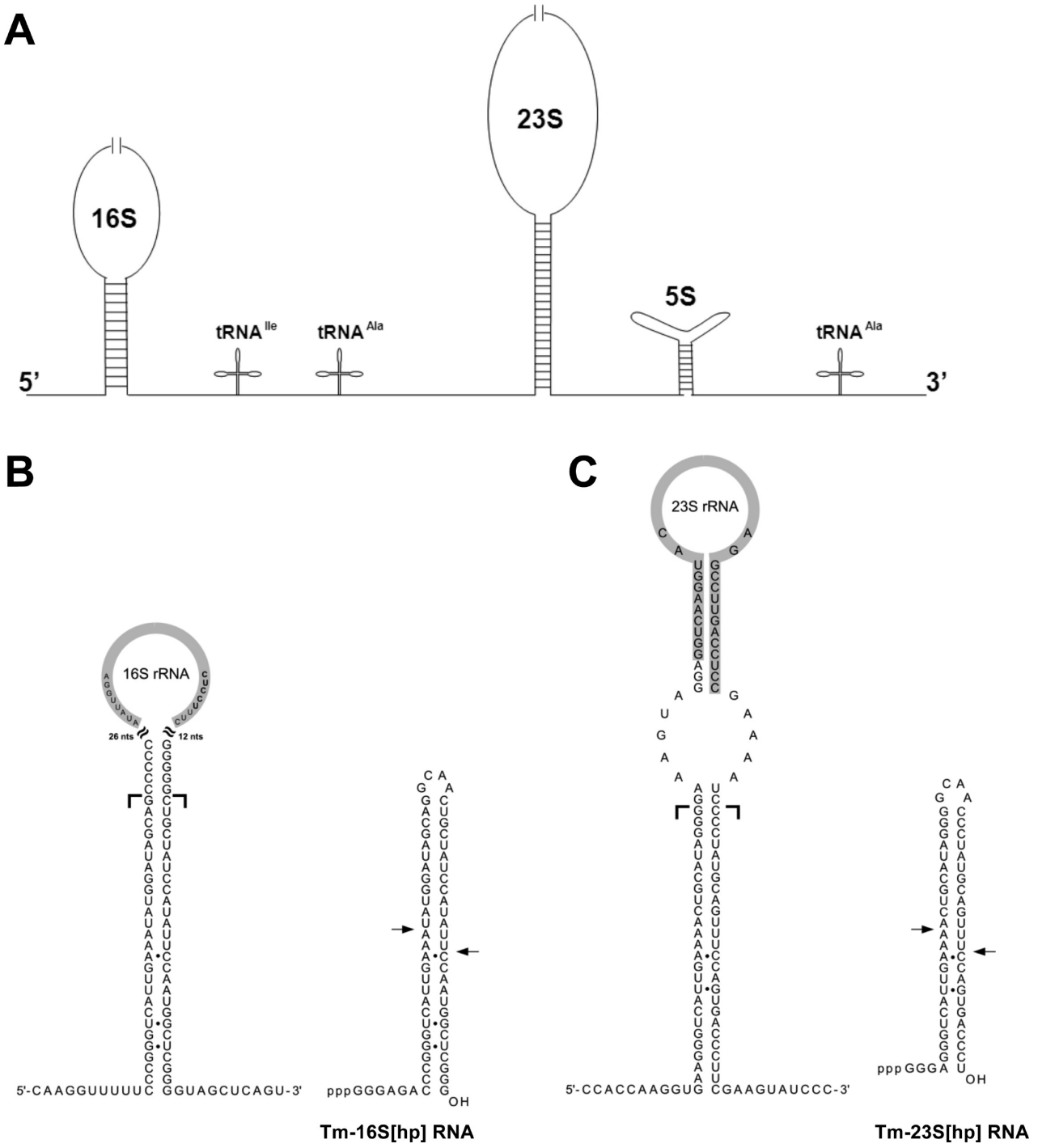

FIGURE 5: Sequences and structures of hairpin substrates based on the *T. maritima* 16S and 23S pre-rRNA stem structures. (A) Schematic structure of the proposed primary transcript of the single rRNA operon of *T. maritima* (estimated length ~5000 nt). The figure is not drawn to scale but highlights the base-paired stems associated with the 16S and 23S rRNA sequences, as well as the positions of the three tRNAs and 5S rRNA. (B) Sequence and proposed secondary structure of the 16S pre-rRNA processing stem (left) and the corresponding hairpin substrate, Tm-16S[hp] RNA (right). The positions of the 5′ and 3′ termini of mature 16S rRNA are indicated by gray highlighting, and the brackets indicate the ends of the double-helical segment incorporated into Tm-16S[hp] RNA. The mapped RNase III cleavage sites in Tm-16S[hp] RNA (see Results) are indicated by arrows. (C) Sequence and proposed secondary structure of the 23S pre-rRNA processing stem (left) and the corresponding hairpin substrate, Tm-23S[hp] RNA (right). Indicated by gray highlighting are the positions of the mature 5′ and 3′ termini of the 23S rRNA, and the brackets indicate the ends of the double-helical segment incorporated into Tm-23S[hp] RNA. The mapped RNase III cleavage sites in Tm-23S[hp] RNA (see Results) are indicated by arrowheads on the right.

products of cleavage by P1 nuclease at pH 9 (G,A-specific), RNase T1 (G-specific), and alkaline pH (Supporting Information Figure 1). The mapped cleavage sites are shown by arrows in Figure 5B,C and reveal that Tm-RNase III cleaves Tm-16S[hp] RNA and Tm-23S[hp] RNA at similar positions. The two sites do not correspond to the mature rRNA 5′ and 3′ termini (Figure 5B,C).

The affinity of Tm-RNase III for Tm-16S[hp] RNA and Tm-23S[hp] RNA was determined by gel mobility shift assays. The binding reactions included Ca^{2+}, which enhances substrate binding to Ec-RNase III but does not support catalysis (*54*) (see also above). 5′-^{32}P-labeled RNA was incubated with increasing amounts of Tm-RNase III, and the reactions were

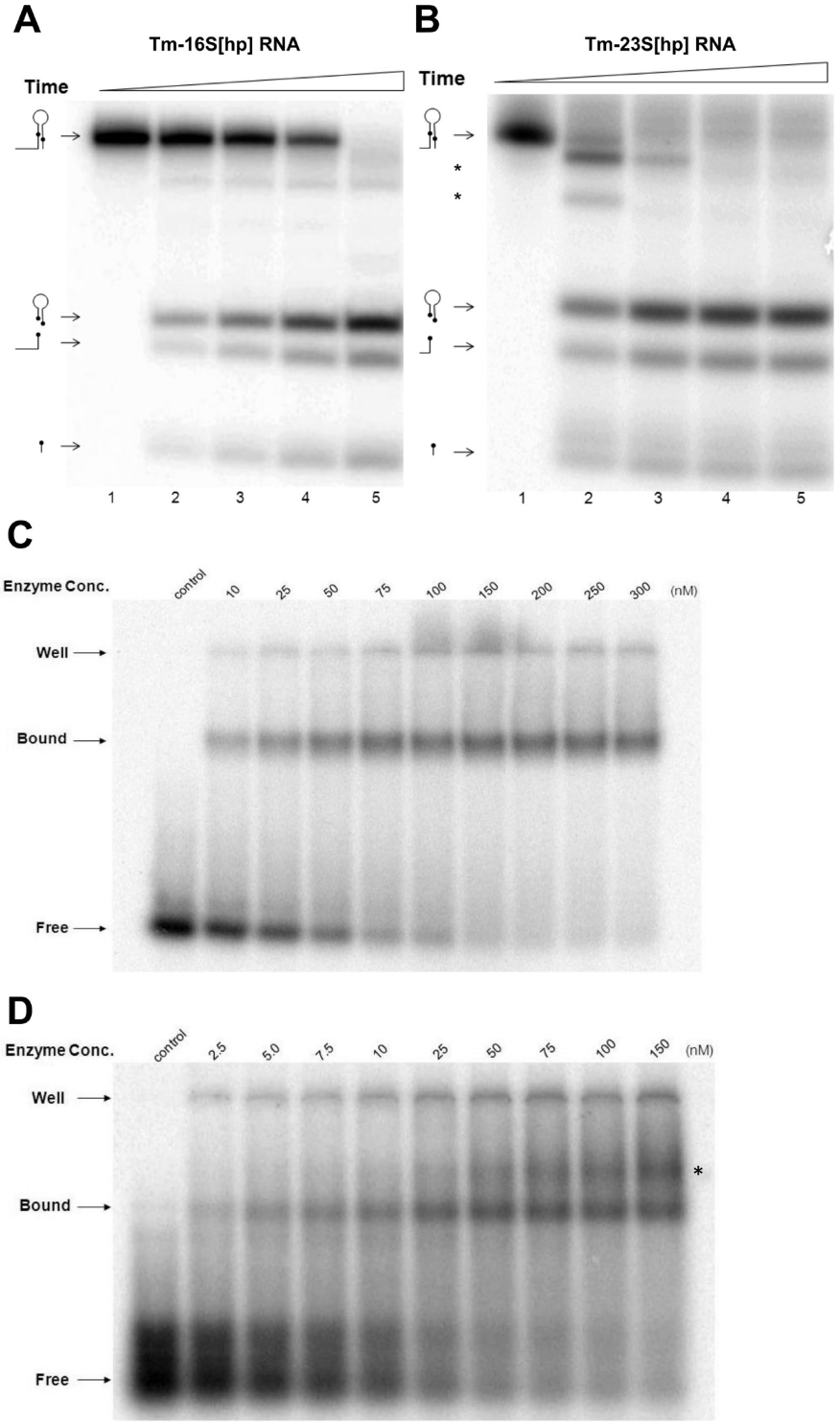

FIGURE 6: Specificity in Tm-RNase III cleavage and binding of Tm-16S[hp] RNA and Tm-23S[hp] RNA. (A) Time course for cleavage of internally ^{32}P-labeled Tm-16S[hp] RNA by Tm-RNase III. Reaction conditions are described in Experimental Procedures. The RNA concentration was 109 nM, and the Tm-RNase III concentration was 25 nM. Lanes 2−5 represent reaction times of 1, 2.5, 5, and 10 min, respectively. Lane 1 represents incubation of substrate with enzyme for 10 min in the absence of Mg^{2+}. The figures on the left side of the phosphorimage represent (from top to bottom) substrate, shortened hairpin product, 5′-end-containing product, and 3′-end-containing product. (B) Time course for cleavage of internally ^{32}P-labeled Tm-23S[hp] RNA by Tm-RNase III. The RNA concentration was 128 nM, and the Tm-RNase III concentration was 25 nM. Lanes 2−5 represent reaction times of 1, 2.5, 5, and 10 min, respectively. Lane 1 represents incubation of substrate with enzyme for 10 min in the absence of Mg^{2+}. See (A) for explanation of the figures on the left side of the phosphorimage. (C) Tm-RNase III binding to 5′-^{32}P-labeled Tm-16S[hp] RNA. Gel shift assays were performed as described in Experimental Procedures. 5′-^{32}P-labeled RNA (2×10^4 dpm; 3 fmol) was incubated with the specified amount of Tm-RNase III in binding buffer and then electrophoresed at 100 V for 3−4 h at ~5 °C in an 8% nondenaturing polyacrylamide gel containing TBE buffer. Reactions were visualized by phosphorimaging. Enzyme concentrations are provided on top of the gel image. The positions of the free and protein-bound RNAs are indicated on the left, along with the position of the wells. (D) Tm-RNase III binding to 5′-^{32}P-labeled 23S[hp] RNA. The experiment was performed as described above. The positions of the free and protein-bound RNAs are indicated on the left, along with the position of the wells. The asterisk on the right indicates the position of the additional complex observed at higher protein concentrations.

electrophoresed in a nondenaturing polyacrylamide gel. Representative assays for each RNA are shown in Figure 6C,D. In each case, a single major complex is observed in the presence of Tm-RNase III, which is consistent with a single target site for cleavage in each RNA. Determination of the apparent dissociation constant (K'_d) for each complex yields values of 16 and 120 nM for the complexes involving Tm-16S[hp] RNA and Tm-23S[hp] RNA, respectively (Supporting Information Figure 2). For Tm-23S[hp] RNA, a second complex of slower mobility is observed at the higher Tm-RNase III concentrations (Figure 6D), indicating the presence of an additional, weaker binding site for Tm-RNase III (see also Discussion).

The Proximal Box Is a Primary Reactivity Epitope for Tm-23S[hp] RNA. Ec-RNase III cleavage sites are determined by two double-helical sequence elements termed the proximal box (pb) and distal box (db) (*55*, *56*). Crystallographic studies of *A. aeolicus* RNase III bound to dsRNA reveal the pb and db as sites of protein contact (*35*, *45*). We thus sought to determine whether the pb and the db also are functional elements in Tm-RNase III substrates. A set of variants of Tm-23S[hp] RNA were prepared that contained single bp substitutions at each of the 14 positions spanning the target site and the terminal tetraloop, including the pb and db positions (Figure 7A). In addition, the GCAA tetraloop sequence was altered to UUUU to assess potential sequence requirements for this structure. Time course cleavage assays were performed using internally ^{32}P-labeled RNA under multiple-turnover (substrate excess) conditions. Short reaction times were used to limit cleavage of substrate to $<\sim$20%, and the relative reactivity of each variant was determined as the ratio of its initial rate of cleavage to that of Tm-23S[hp] RNA. Representative assays are shown in Figure 7B, and the relative reactivities of all of the variants are provided in Figure 7A. A relative reactivity $<\sim$0.5 was regarded as reflecting a significant effect of a given bp substitution. The data reveal that the majority of the bp substitutions have minor effects on reactivity and that there is no strict tetraloop sequence requirement. Significantly, substitutions in the distal box position have relatively minor effects on reactivity, with even the structurally disruptive GG mismatch at db position 2 causing only a modest reduction in reactivity (Figure 7A).

Substitutions at pb positions 2 and 4 have significant effects on cleavage reactivity (panels B and C of Figure 7, respectively). Thus, a CG or GC bp substitution at pb position 2 reduces the relative reactivity to 0.1 and 0.3, respectively, while a CG or GC substitution at pb position 4 provides a relative reactivity of 0.1 or 0.4, respectively. At pb position 3, only the AU bp substitution causes a significant drop in relative reactivity (0.3), while none of the bp substitutions at pb position 1 has a significant effect. We conclude that the pb is the primary element in Tm-23S[hp] RNA that controls reactivity, with positions 2, 3, and 4 the most sensitive to specific bp substitution. The inset in Figure 7A summarizes the preferred sequences in the pb. A loss of reactivity may reflect either an inhibition of enzyme binding or an inhibition of the cleavage step. In the former case, the inhibitory bp functions as a recognition antideterminant, while in the latter case it acts as a catalytic antideterminant (*56*). To determine the mode of bp inhibition, a gel shift assay was performed on the two minimally reactive Tm-23S[hp] RNA variants. The data in Figure 8 reveal that a GC bp substitution at pb position 2 (Figure 8A) or position 4 (Figure 8B) does not significantly affect binding of Tm-RNase III to the RNA. These results indicate that the CG bp at pb positions 2 or 4 functions as a catalytic antideterminant.

Tm-RNase III Accurately Cleaves a Substrate of a Phylogenetically Distant RNase III. *T. maritima* occupies a deeply branching portion of the bacterial phylogenetic tree that is distant from the lineage that includes *E. coli* (*3*, *4*). The similarity of the consensus pb sequence for Ec- and Aa-RNase III substrates (see Figure 7 inset) prompted the question whether Tm-RNase III can cleave an Ec-RNase III substrate in a similar manner. R1.1 RNA and R1.1[WC-R] RNA (Figure 9A,B) were selected as representative Ec-RNase III substrates. R1.1 RNA is based on the R1.1 processing signal in the T7 coliphage early region (*57*) and contains a single scissile bond within the asymmetric internal loop (*57*, *58*). R1.1[WC-R] RNA is a synthetic variant of R1.1 RNA that has a regular double-helical structure, and two phosphodiesters are cleaved at the target site (*59*). A time course assay (Figure 9C) shows that Tm-RNase III cleaves R1.1[WC-R] RNA with the same specificity as Ec-RNase III. The reciprocal experiment shows that Ec-RNase III cleaves Tm-23S[hp] RNA and Tm-16S[hp] RNA at the Tm-RNase III cleavage sites (Figure 9E,F), but several additional sites are cleaved as well, suggesting a less stringent specificity of Ec-RNase III with respect to target site selection. The essentially identical cleavage patterns for R1.1[WC] RNA show that Tm-RNase III recognizes Ec-RNase III substrate reactivity epitopes. The inability of Tm-RNase III to cleave R1.1 RNA (Figure 9D), however, suggests that Tm-RNase III substrates may be limited to regular double-helical structures.

DISCUSSION

This study has characterized the biochemical properties of RNase III from *T. maritima* and demonstrated the conservation of substrate reactivity epitopes over a broad phylogenetic distance. Mg^{2+} best supports catalytic activity, which is consistent with the emerging consensus that Mg^{2+} is the physiologically relevant cofactor for RNase III family members (*60*, *61*). Mn^{2+} ion also supports activity, albeit to a lesser extent, but in contrast to Ec-RNase III (*62*, *63*), higher Mn^{2+} concentrations are not inhibitory. However, Co^{2+} inhibits as well as supports Tm-RNase III catalytic activity in a manner similar that seen with Mn^{2+} and Ec-RNase III (*62*, *63*). One possibility is that Co^{2+} at higher concentrations can occupy a binding site on the enzyme, as proposed for Ec-RNase III (*62*, *63*), and cause inhibition. However, a direct interaction of Co^{2+} with RNA cannot be ruled out. Tm-RNase III is most active at salt concentrations in the $\sim$50−80 mM range, with higher concentrations causing inhibition. Ec-RNase III is most active at salt concentrations $>\sim$150 mM, with lower concentrations promoting cleavage of additional (secondary) sites, which are not recognized *in vivo* (*58*, *60*). In contrast, neither *Thermotoga* substrate was cleaved at sites other than the primary sites over the examined salt concentrations. Tm-RNase III exhibits a transition to greater activity between pH 7 and pH 8, with the midpoint of the transition indicating ionization of one or more groups with an apparent pK_a of $\sim$7.5. This behavior could reflect conversion of the metal-bound water nucleophile to the more reactive form (*64*). However, since it was shown for Ec-RNase III that product release, rather than the chemical step, is rate-limiting in the steady state (*64*), a more likely possibility is that the higher pH facilitates product release. One interpretation is that an increase in negative charge on the protein surface destabilizes the binding of the (anionic) cleavage products.

Tm-RNase III exhibits optimal activity at temperatures from $\sim$40 to 70 °C, with significant activity retained at 95 °C. It is

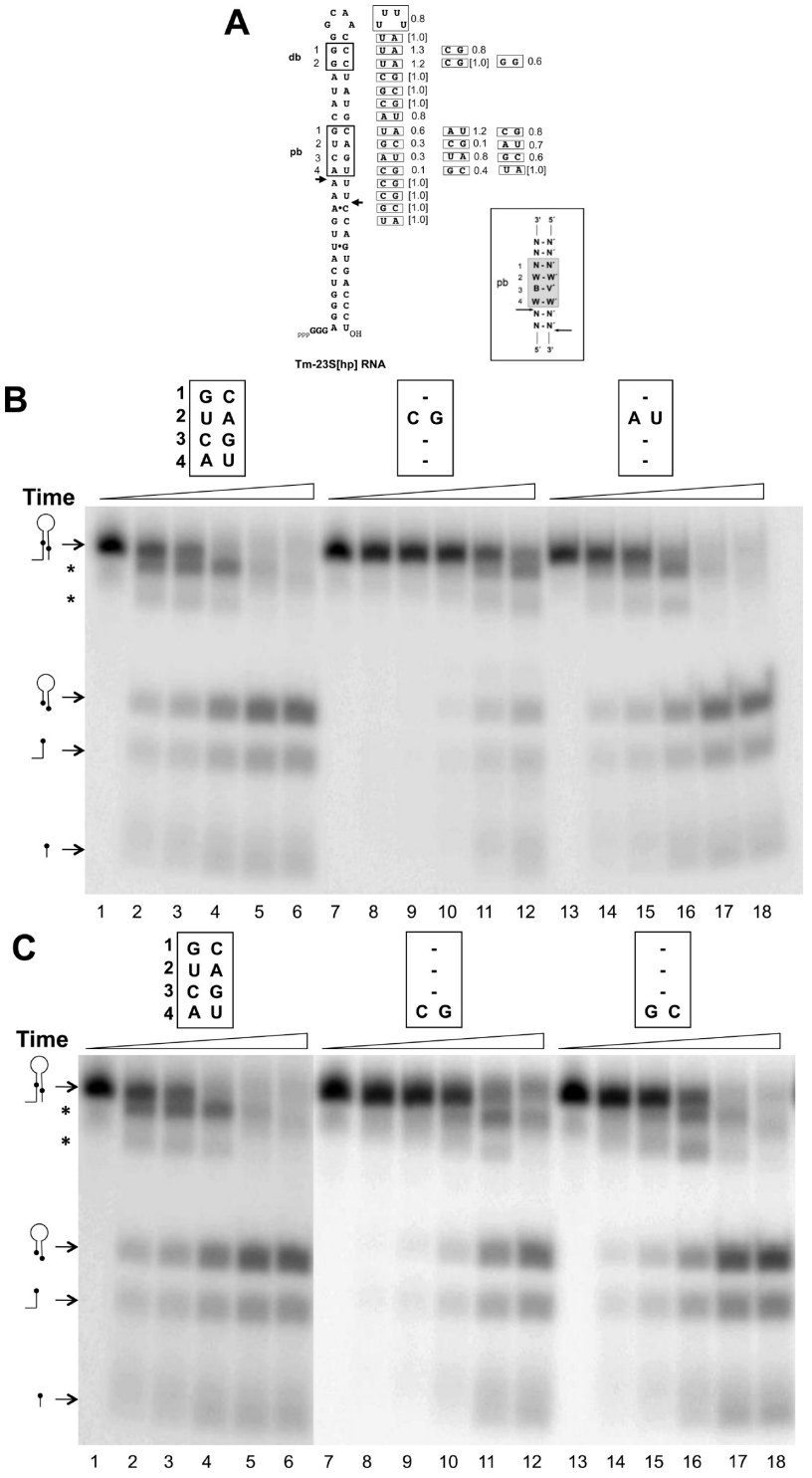

FIGURE 7: Base-pair sequence control of Tm-23S[hp] RNA reactivity. (A) Sequences and relative reactivities of variants of Tm-23S[hp] RNA. The positions of the proximal box (pb) and distal box (db) are indicated, and scissile bonds are indicated by arrows. The calculated relative reactivities are provided next to the bp substitutions. Assays were done in duplicate for the variants that showed significant differences in activity (> 0.2 change in relative reactivity). Values within brackets indicate a reactivity essentially indistinguishable from the parent substrate, with the brackets indicating only a single measurement was made. Inset: Proposed consensus for the proximal box. W−W′ refers to AU or UA bp, B refers to G, U, or C (not A), and V′ refers to a nucleotide (not U) that is complementary to B. N−N′ is any standard base pair. RNase III scissile bonds are indicated by arrows. (B) Reactivities of Tm-23S[hp] RNA variants containing a UA → CG or UA → AU bp substitution at pb position 2. Cleavage reactions were performed as described in Experimental Procedures using internally ^{32}P-labeled RNA (128 nM) and Tm-RNase III (25 nM). Reactions were initiated by adding RNA, followed by incubation at 45 °C for the specified times. Lanes 2−6, 8−12, and 14−19 represent 15 s, 30 s, 1 min, 2.5 min, and 5 min reaction times, respectively, for each RNA. Lanes 1, 7, and 13 are control reactions in which RNA was incubated with enzyme for 5 min in the absence of Mg^{2+}. The positions of the substrate and the three cleavage products are indicated, and the asterisks indicate the positions of the single-cleaved intermediates. (C) Reactivities of Tm-23S[hp] RNA variants containing an AU → CG or AU → GC bp substitution at pb position 1. Cleavage reactions were performed as described above. Lanes 2−6, 8−12, and 14−19 represent 15 s, 30 s, 1 min, 2.5 min, and 5 min reaction times, respectively, for each RNA. Lanes 1, 7, and 13 are control reactions in which RNA was incubated with enzyme for 5 min in the absence of Mg^{2+}. The positions of the substrate and the three cleavage products are indicated.

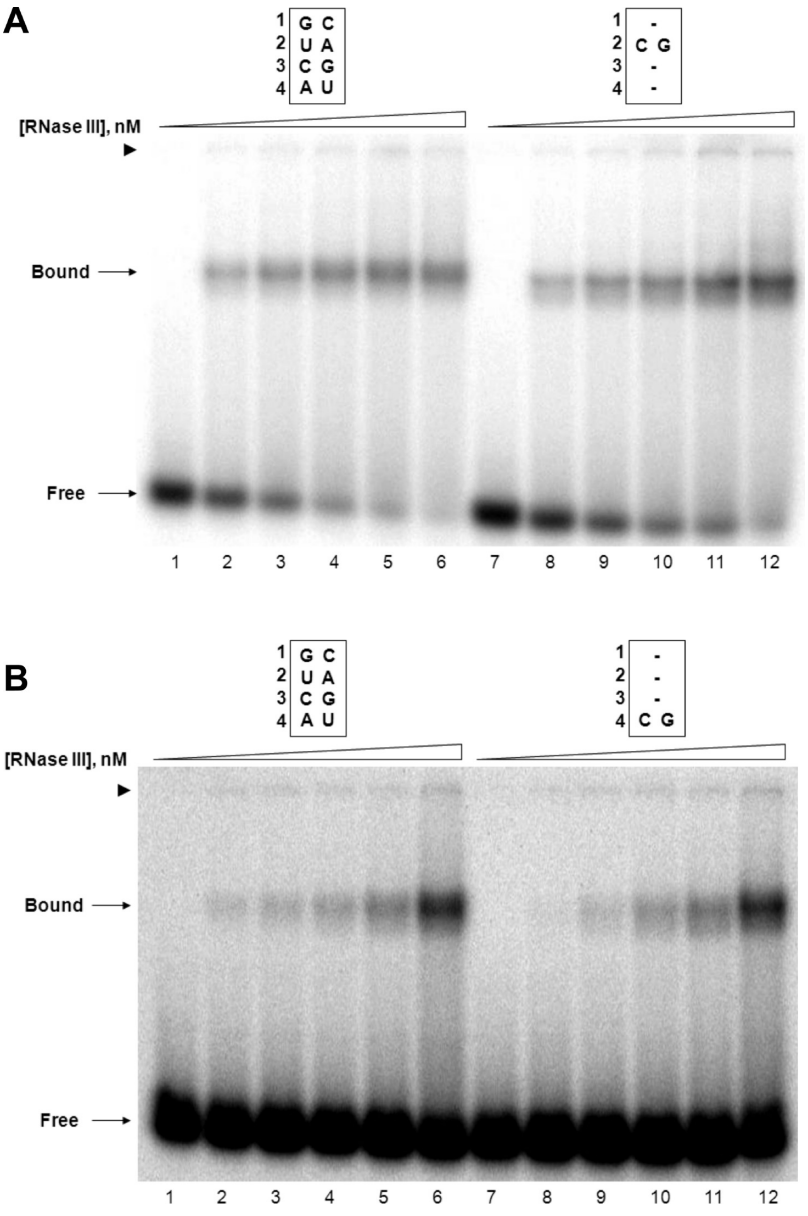

FIGURE 8: Proximal box bp substitutions at positions 2 and 4 act as catalytic antideterminants. Gel shift assays were performed using 5′-^{32}P-labeled RNA, as described in Experimental Procedures. (A) The UA → CG substitution at pb position 2 does not affect binding affinity. In lanes 2−6 and 8−12, the Tm-RNase III concentrations are 10, 25, 50, 100, and 150 nM (dimer concentration). Lanes 1 and 7 are reactions that lack enzyme. (B) The AU → CG substitution at pb position 4 does not affect binding affinity.

possible that the drop in activity at temperatures > 90 °C reflects denaturation of RNA rather than protein. A correlation has been noted between protein thermostability and the charged versus polar (C*v*P) bias, which is the difference between the percentage of charged residues (Asp, Glu, Lys, Arg) and polar residues (Asn, Gln, Thr, Ser) in a polypeptide (*65*, *66*). A higher CvP-bias value reflects an increase in the number of salt bridges that contribute to thermostability and an avoidance of thermolabile Asn and Gln residues (*65*, *66*). The C*v*P bias for Tm-RNase III is 19.17, which is significantly higher than the value of 5.75 for Ec-RNase III. These values also can be compared to the average C*v*P bias values of 13.23 and 2.63 for *T. maritima* and *E. coli* proteins, respectively (*66*). In addition, through pairwise comparisons of the structures of *T. maritima* proteins with their mesophile counterparts, a direct correlation was noted between thermostability and contact order (CO) (*7*, *8*). We used the 2.0 Å Tm-RNase III structure (PDB entry 1O0W) and the 2.1 Å structure of RNase III of the mesophile *M. tuberculosis* (Mt) (PDB entry 2A11) to calculate the respective CO values. The relative CO for Tm-RNase III (normalized to chain length) is 0.057, which is lower than the Mt-RNase III value of 0.093, indicating that contact order does not contribute to Tm-RNase III thermostabilty.

The site-specific action of Tm-RNase III was demonstrated using RNA hairpins based on the *Thermotoga* 16S and 23S pre-rRNA processing stems. The target sites are consistent with the observation of a single RNA−protein complex in a nondenaturing polyacrylamide gel and support a role for RNase III in providing the immediate precursors to the mature rRNAs. The functional relevance, if any, of the second complex observed with Tm-23S[hp] RNA is not known. The K'_d values differ for the complexes involving Tm-16S[hp] RNA and Tm-23S[hp] RNA, with the Tm-RNase III−Tm-16S[hp] RNA complex exhibiting a significantly lower K'_d. The greater stability of this complex may reflect the longer stem length of Tm-16S[hp] RNA that would maximize the number of protein−RNA contacts. Although Tm-16S[hp] RNA is bound more tightly by Tm-RNase III than

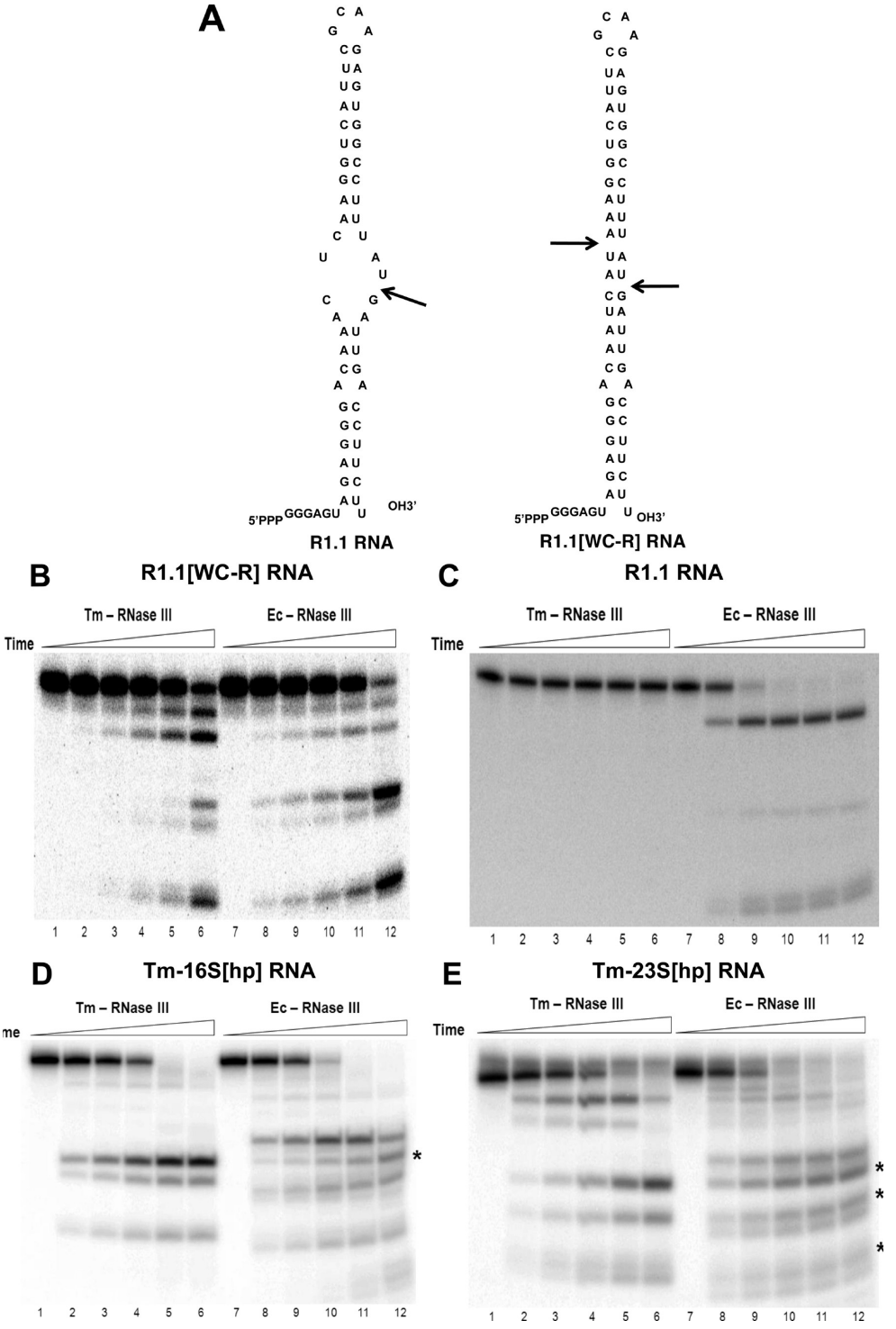

FIGURE 9: Tm-RNase III cleavage of Ec-RNase III substrates. (A) Structure of R1.1 RNA and R1.1[WC-R] RNA. The arrows indicate the Ec-RNase III cleavage sites. (B) Tm-RNase III cleavage of internally ^{32}P-labeled R1.1[WC-R] RNA (90 nM). Time course assays of RNA cleavage assays were performed as described in Experimental Procedures. Lanes 2−6 and lanes 8−12 represent reaction times of 1, 2.5, 5, 10, and 30 min for Tm-RNase III (10 nM) and Ec-RNase III (10 nM), respectively. Lanes 1 and 7 represent control reactions where RNA was incubated in buffer for 1 min in the absence of enzyme. (C) Tm-RNase III does not cleave R1.1 RNA. Reactions were performed using internally ^{32}P-labeled R1.1 RNA (96 nM), using the standard reaction buffer as described in Experimental Procedures. Lanes 2−6 and lanes 8−12 represent reaction times of 1, 2.5, 5, 10, and 30 min with Tm-RNase III (10 nM) and Ec-RNase III (10 nM), respectively. Lanes 1 and 7 represent control reactions where RNA was incubated with enzyme for 1 min in the absence of enzyme. (D) Ec-RNase III cleavage of internally ^{32}P-labeled Tm-16S[hp] RNA (109 nM). Lanes 2−6 and lanes 8−12 represent 1, 2.5, 5, 10, and 30 min reaction times with Tm-RNase (10 nM) and Ec-RNase III (10 nM), respectively. Lanes 1 and 8 represent control reactions where RNA was incubated in buffer for 1 min in the absence of enzyme. The asterisk on the right indicates the Ec-RNase III cleavage product with identical gel electrophoretic mobility as a Tm-RNase III reaction product. (E) Ec-RNase III cleavage of internally ^{32}P-labeled Tm-23S[hp] RNA (128 nM). Lanes 2−6 and lanes 8−12 represent 1, 25, 5, 10, and 30 min reaction times with Tm-RNase III (10 nM) and Ec-RNase III (10 nM), respectively. Lanes 1 and 7 show control reactions where RNA was incubated for 1 min in buffer in the absence of enzyme. Asterisks on the right indicate Ec-RNase III cleavage products with identical gel electrophoretic mobilities as products in the Tm-RNase III reaction. It is important to note that the denaturing gels used in these analyses are able to detect single nt differences in electrophoretic mobilities of RNAs in this size range (*55*, *56*).

Tm-23S[hp] RNA, it is cleaved more slowly. We note that a longer stem length also reduced the reactivity of an Ec-RNase III substrate (*56*). Since the cleavage assays were performed using conditions of substrate excess, a slower product release step for Tm-16S[hp] cleavage, which would also be reflected in a higher affinity for substrate, would provide a slower overall rate. A similar behavior has been noted with Ec-RNase III cleavage of the two cognate substrates, R1.1 RNA and R1.1[WC] RNA (*54*). Whether the differing reactivities are maintained *in vivo* is not known, but it is likely that other cellular factors contribute to *in vivo* reactivity.

Reactivity epitopes for Ec-RNase III substrates include structural features such as internal loops, which restrict cleavage to one strand (*67*), and a double-helical length requirement of ≥11 bp (*56*). However, Tm-RNase III does not efficiently cleave an internal loop-containing substrate of Ec-RNase III nor cognate RNA hairpins with stem lengths less than ~21 bp. In both cases the lack of reactivity is due to a loss of binding affinity (L. Nathania and A. W. Nicholson, unpublished experiments). Tm-RNase III substrates may require two turns of a regular double helix in order for both dsRBDs and the nuclease domain to engage substrate. However, the length requirement is not a consequence of protein thermostability *per se*, since the comparably thermostable *A. aeolicus* RNase III can cleave substrates with short (~11 bp) stems (Z. Shi, R. H. Nicholson, R. Jaggi, and A. W. Nicholson, submitted).

The proximal box is a key functional element in Tm-RNase III substrates and exhibits a consensus sequence that is similar to that of the pb for Ec-RNase III substrates (see Figure 7 inset). Such a consensus pb would specify a cleavage site every ~5 bp in a random sequence dsRNA. However, this degeneracy would not necessarily compromise attainment of the necessary specificity if the pb occurs within a limited-length double-helical segment. Tm-RNase III, like Ec-RNase III, is sensitive to bp antideterminants, which have been proposed to protect functionally important double-helical RNA structures from unwanted cleavage (*55*). For Tm-RNase III, a GC or CG bp substitution at pb position 2 or 4 inhibits reactivity in a manner similar to that observed with the same substitutions at the same positions in an Ec-RNase III substrate (*56*). For Tm-RNase III, these substitutions inhibit cleavage without blocking enzyme binding and therefore act as catalytic antideterminants (*56*). Crystal structures of *A. aeolicus* RNase III bound to dsRNA reveal that the pb interacts with the N-terminal α-helix of the dsRBD, termed RBM1, and which contains several highly conserved residues whose side chains contact the pb minor groove (*35*, *45*). Mutational analyses underway should enable definition of the energetic contribution of the conserved side chains to substrate binding and also gain further insight on modes of antideterminant action. The distal box is a 2 bp element that was first identified in Ec-RNase III substrates (*55*, *56*) and was shown in Aa-RNase III-dsRNA cocrystal structures to interact with a nonconserved region in the nuclease domain, termed RBM4 (Figure 1C) (*35*, *45*). In contrast to Ec-RNase III substrates, bp substitutions in the db of Tm-23S[hp] RNA do not significantly affect reactivity. The absence of a db sequence effect on reactivity may be related to the variability in RBM4 sequence and length. Thus, while the db-RBM4 interaction is conserved, it may be largely limited to bp-sequence-independent interactions with the sugar−phosphate backbone. In turn, this would support a primary role for the db in substrate recognition that is sensitive to dsRNA length [as also noted elsewhere (*35*)] rather than bp sequence.

The other ribonucleases involved in *Thermotoga* 16S and 23S rRNA maturation have not been identified but may include RNase E/G and the 3′→5′ exonucleases RNase R and/or PNPase (*9*, *33*, *34*). RNase E/G action may also provide the mature 5S rRNA, and the three tRNAs could be matured in two endonucleolytic steps, involving 5′-end formation by RNase P (*10*) and 3′-end formation by tRNase Z, acting at a site directly downstream of the encoded CCA sequence (*15*). Since *in vitro* reactions using purified bacterial RNases III and model substrates accurately reflect *in vivo* processing behavior (*16*, *19*, *57*, *60*, *61*), and since the pre-rRNA stems are conserved targets for bacterial RNases III, the approach described in this paper provides a general method to characterize RNase III processing of other bacterial rRNA precursors and to identify additional cellular substrates. While *T. maritima* is not an especially accessible organism for genetic and physiological studies, the *Thermotoga* protein database has been used in a recent analysis of the structural basis for central metabolic network function (*68*). It can be anticipated that structural and biochemical studies of purified *Thermotoga* ribonucleases and their substrates may provide a similar, integrated structure−function understanding of bacterial RNA processing and decay networks.

ACKNOWLEDGMENT

We thank Francis Jenney (University of Georgia) for the gift of *T. maritima* DNA. We also thank Xinhua Ji, Don Court, and Rhonda Nicholson for comments on the manuscript and other members of the laboratory for advice and encouragement.

SUPPORTING INFORMATION AVAILABLE

Mapping of Tm-RNase III cleavage sites in Tm-16S[hp] RNA and Tm-23S[hp] RNA (Figure S1), determination of the K'_d values for the Tm-RNase III complexes involving Tm-16S[hp] RNA and Tm-23S[hp] RNA (Figure S2), and legends providing the experimental details and references. This material is available free of charge via the Internet at http://pubs.acs.org.

REFERENCES

1. Deutscher, M. P. (2006) Degradation of RNA in bacteria: comparison of mRNA and stable RNA. *Nucleic Acids Res. 34*, 659–666.
2. Condon, C. (2007) Maturation and degradation of RNA in bacteria. *Curr. Opin. Microbiol. 10*, 271–278.
3. Nelson, K. E., Clayton, R. A., Gill., S. R., Gwinn, M. L., and Dodson, R. J.; et al. (1999) Evidence for lateral gene transfer between Archaea and Bacteria from the genome sequence of *Thermotoga maritima*. *Nature 399*, 323–329.
4. Zhaxybayeva, O., Swithers, K. S., Lapierre, P., Fournier, G. P., Bickhart, D. M., DeBoy, R. T., Nelson, K. E., Nesbe, C. L., Doolittle, W. F., Gogarten, J. P., and Noll, K. M. (2009) On the chimeric nature, thermophilic origin, and phylogenetic placement of the Thermotogales. *Proc Natl. Acad. Sci. U.S.A. 106*, 5865–5870.
5. Didonato, M., Deacon, A. M., Klock, H. E., McMullan, D., and Lesley, S. A. (2004) A scaleable and integrated crystallization pipeline applied to mining the *Thermotoga maritima* proteome. *J. Struct. Funct. Genomics 5*, 133–146.
6. Canaves, J. M., Page, R., Wilson, I. A., and Stevens, R. C. (2004) Protein biophysical properties that correlate with crystallization success in *Thermotoga maritima*: maximum clustering strategy for structural genomics. *J. Mol. Biol. 344*, 977–991.
7. Robinson-Rechavei, M., and Godzik, A. (2005) Structural genomics of *Thermotoga maritima* proteins shows that contact order is a major determinant of protein thermostability. *Structure* (*Cambridge*) *13*, 857–860.
8. Robinson-Rechavi, M., Alibés, A., and Godzik, A. (2006) Contribution of electrostatic interactions, compactness and quaternary structure to protein thermostability: lessons learned from structural genomics of *Thermotoga maritima*. *J. Mol. Biol. 356*, 547–557.

9. Condon, C., and Putzer, H. (2002) The phyogenetic distribution of bacterial ribonucleases. *Nucleic Acids Res. 30*, 5339–5346.
10. Paul, R., Lazarev, D., and Altman, S. (2001) Characterization of RNase P from *Thermotoga maritima*. *Nucleic Acids Res. 29*, 880–885.
11. Kazantsev, A. V., Krivenko, A. A., Harrington, D. J., Carter, R. J., Holbrook, S. R., Adams, P. D., and Pace, N. R. (2003) High-resolution structure of RNase P protein from *Thermotoga maritima*. *Proc. Natl. Acad. Sci. U.S.A. 100*, 7497–7502.
12. Torres-Larios, A., Swinger, K. K., Krasilnikov, A. S., Pan, T., and Mondragon, A. (2005) Crystal structure of the RNA component of bacterial ribonuclease P. *Nature 437*, 584–587.
13. Ishii, R., Minagawa, A., Takaku, H., Takagi, M., Nashimoto, M., and Yokoyama, S. (2005) Crystal structure of the tRNA 3′ processing endoribonuclease tRNase Z from *Thermotoga maritima*. *J. Biol. Chem. 280*, 14138–14144.
14. Minagawa, A., Takaku, H., Ishii, R., Takagi, M., Yokoyama, S., and Nashimoto, M. (2006) Identification by Mn^{2+} rescue of two residues essential for the proton transfer of tRNase Z catalysis. *Nucleic Acids Res. 34*, 3811–3818.
15. Minagawa, A., Takaku, H., Takagi, M., and Nashimoto, M. (2004) A novel endonucleolytic mechanism to generate the CCA 3′ termini of tRNA molecules in *Thermotoga maritima*. *J. Biol. Chem. 279*, 15688–15697.
16. Court, D. L. (1993) RNA processing and degradation by RNase III, in Control of Messenger RNA Stability (Belasco, J. G., and Brawerman, G., Eds.) pp 71−116, Academic Press, New York.
17. LaMontagne, B., Larose, S., Boulanger, J., and AbouElela, S. (2001) The RNase III family: a conserved structure and expanding functions in eukaryotic dsRNA metabolism. *Curr. Issues Mol. Biol. 3*, 71–78.
18. Conrad, C., and Rauhut, R. (2002) Ribonuclease III: new sense from nuisance. *Int. J. Biochem. Cell Biol. 34*, 116–129.
19. Nicholson, A. W. (2003) The ribonuclease III superfamily: forms and functions in RNA maturation, decay, and gene silencing, in RNAi: A Guide to Gene Silencing (Hannon, G. J., Ed.) pp 149−174, Cold Spring Harbor Laboratory Press, Cold Spring Harbor, NY.
20. Drider, D., and Condon, C. (2004) The continuing story of endoribonuclease III. *J. Mol. Microbiol. Biotechnol. 8*, 195–200.
21. MacRae, I. J., and Doudna, J. A. (2007) Ribonuclease revisited: structural insights into ribonuclease III family enzymes. *Curr. Opin. Struct. Biol. 17*, 138–145.
22. Ji, X. (2008) The mechanism of RNase III action: how dicer dices. *Curr. Top. Microbiol. Immunol. 320*, 99–116.
23. Price, B., Adamidis, T., Kong, R., and Champness, W. (1999) A *Streptomyces coelicolor* antibiotic regulatory gene, absB, encodes an RNase III homolog. *J. Bacteriol. 181*, 6142–6151.
24. Gravenbeek, M. L., and Jones, G. H. (2008) The endonuclease activity of RNase III is required for the regulation of antibiotic production by *Streptomyces coelicolor*. *Microbiology 154*, 3547–3555.
25. Sello, J. K., and Buttner, M. J. (2008) The gene encoding RNase III in *Streptomyces coelicolor* is transcribed during exponential phase and is required for antibiotic production and for proper sporulation. *J. Bacteriol. 190*, 4079–4083.
26. Xu, W., Huang, J., Lin, R., Shi, J., and Cohen, S. N. (2010) Regulation of morphological differentiation in *S. coelicolor* by RNase III (AbsB) cleavage of mRNA encoding the AdpA transcription factor. *Mol. Microbiol. 75*, 781–791.
27. Huntzinger, E., Boisset, S., Saveanu, C., Benito, Y., Geissmann, T., Namane, A., Lina, G., Etienne, J., Ehresmann, B., Ehresmann, C., Jacquier, A., Vandenesch, F., and Romby, P. (2005) *Staphylococcus aureus* RNAIII and the endoribonuclease III coordinately regulate *spa* gene expression. *EMBO J. 24*, 824–835.
28. Saito, H., and Richardson, C. C. (1981) Processing of mRNA by ribonuclease III regulates expression of gene 1.2 of bacteriophage T7. *Cell 27*, 533–542.
29. Schmeissner, U., McKenney, K., Rosenberg, M., and Court, D. (1984) Removal of a terminator structure by RNA processing regulates *int* gene expression. *J. Mol. Biol. 176*, 39–53.
30. Krinke, L., Mahoney, M., and Wulff, D. L. (1991) The role of the OOP antisense RNA in coliphage lambda development. *Mol. Microbiol. 5*, 1265–1272.
31. Gerdes, K., Nielsen, A., Thorsted, P., and Wagner, E. G. (1992) Mechanism of killer gene activation. Antisense RNA-dependent RNase III cleavage ensures rapid turn-over of the stable hok, srnB and pndA effector messenger RNAs. *J. Mol. Biol. 226*, 637–649.
32. Saito, R., Ozawa, Y., Kuzuno, N., and Tomita, M. (2000) Computer analysis of potential stem structures of rRNA operons in various procaryotic genomes. *Gene 259*, 217–222.
33. Srivastava, A., and Schlessinger, D. (1990) Mechanism and regulation of bacterial ribosomal RNA processing. *Annu. Rev. Microbiol. 44*, 105–129.
34. Deutscher, M. P. (2009) Maturation and degradation of ribosomal RNA in bacteria. *Prog. Mol. Biol. Transl. Sci. 85*, 369–391.
35. Gan, J., Shaw, G., Tropea, J. E., Waugh, D. S., Court, D. L., and Ji, X. (2008) A stepwise model for double-stranded RNA processing by ribonuclease III. *Mol. Microbiol. 67*, 143–154.
36. MacRae, I. J., Zhou, K., Li, F., Repic, A., Brooks, A. N., Cande, W. Z., Adams, P. D., and Doudna, J. A. (2006) Structural basis for double-stranded RNA processing by Dicer. *Science 311*, 195–198.
37. Sun, W., Pertzev, A., and Nicholson, A. W. (2005) Catalytic mechanism of *Escherichia coli* ribonuclease III. Kinetic and inhibitor evidence for the involvement of two Mg^{2+} ions in phosphodiester hydrolysis. *Nucleic Acids Res. 33*, 807–815.
38. Meng, W., and Nicholson, A. W. (2008) Heterodimer-based analysis of subunit and domain contributions to double-stranded RNA processing by *Escherichia coli* RNase III *in vitro*. *Biochem. J. 410*, 39–48.
39. Conrad, C., Schmitt, J. G., Evguenieva-Hackenberg, E., and Klug, G. (2002) One functional subunit is sufficient for catalytic activity and substrate specificity of *Escherichia coli* endoribonuclease III artificial heterodimers. *FEBS Lett. 518*, 93–96.
40. Redko, Y., Bechhofer, D. H., and Condon, C. (2008) Mini-III, an unusual member of the RNase III family of enzymes, catalyses 23S ribosomal RNA maturation in *B. subtilis*. *Mol. Microbiol. 68*, 1096–1106.
41. Redko, Y., and Condon, C. (2009) Ribosomal protein L3 bound to 23S precursor rRNA stimulates its maturation by mini-III ribonuclease. *Mol. Microbiol. 71*, 1145–1154.
42. Blaszczyk, J., Tropea, J. E., Bubunenko, M., Routzahn, K. M., Waugh, D. S., Court, D. L., and Ji, X. (2001) Crystallographic and modeling studies of RNase III suggest a mechanism for double-stranded RNA cleavage. *Structure 9*, 1225–1236.
43. Blaszczyk, J., Gan, J., Tropea, J. E., Court, D. L., Waugh, D. S., and Ji, X. (2004) Noncatalytic assembly of ribonuclease III with double-stranded RNA. *Structure 12*, 457–466.
44. Gan, J., Tropea, J. E., Austin, B. P., Court, D. L., Waugh, D. S., and Ji, X. (2005) Intermediate states of ribonuclease III in complex with double-stranded RNA. *Structure 13*, 1435–1442.
45. Gan, J., Tropea, J. E., Austin, B. P., Court, D. L., Waugh, D. S., and Ji, X. (2006) Structural insight into the mechanism of double-stranded RNA processing by ribonuclease III. *Cell 124*, 355–366.
46. Akey, D. L., and Berger, J. M. (2005) Structure of the nuclease domain of ribonuclease III from *M. tuberculosis* at 2.1 Å. *Protein Sci. 14*, 2744–2750.
47. Meng, W., Nicholson, R. H., Nathania, L., Pertzev, A. V., and Nicholson, A. W. (2008) New approaches to understanding double-stranded RNA processing by ribonuclease III. Purification and assays of homodimeric and heterodimeric forms of RNase III from bacterial extremophiles and mesophiles. *Methods Enzymol. 447*, 119–129.
48. Amarasinghe, A. K., Calin-Jageman, I., Harmouch, A., Sun, W., and Nicholson, A. W. (2001) *Escherichia coli* ribonuclease III: affinity purification of hexahistidine-tagged enzyme and assays for substrate binding and cleavage. *Methods Enzymol. 342*, 143–158.
49. He, B., Rong, M, Lyakhov, D., Gartenstein, H., Diaz, G., Castagna, R., McAllister, W. T., and Durbin, R. K. (1997) Rapid mutagenesis and purification of phage RNA polymerases. *Protein Expression Purif. 9*, 142–151.
50. Milligan, J. F., Groebe, D. R., Witherell, G. W., and Uhlenbeck, O. C. (1987) Oligoribonucleotide synthesis using T7 RNA polymerase and synthetic DNA templates. *Nucleic Acids Res. 15*, 8783–8798.
51. Milligan, J. F., and Uhlenbeck, O. C. (1989) Synthesis of small RNAs using T7 RNA polymerase. *Methods Enzymol. 180*, 51–62.
52. Peattie, D. A. (1979) Direct chemical method for sequencing RNA. *Proc. Natl. Acad. Sci. U.S.A. 76*, 1760–1764.
53. Carey, J., Cameron, V., deHaseth, P. L., and Uhlenbeck, O. C. (1983) Sequence-specific interaction of R17 coat protein with its ribonucleic acid binding site. *Biochemistry 22*, 2601–2610.
54. Li, H., and Nicholson, A. W. (1996) Defining the enzyme binding domain of a ribonuclease III processing signal. Ethylation interference and hydroxyl radical footprinting using catalytically inactive RNase III mutants. *EMBO J. 15*, 1421–1433.
55. Zhang, K., and Nicholson, A. W. (1997) Regulation of ribonuclease III processing by double-helical sequence antideterminants. *Proc. Natl. Acad. Sci. U.S.A. 94*, 13437–13441.
56. Pertzev, A., and Nicholson, A. W. (2006) Characterization of RNA sequence determinants and antideterminants of processing reactivity for a minimal substrate of *Escherichia coli* ribonuclease III. *Nucleic Acids Res. 34*, 3708–3721.
57. Dunn, J. J., and Studier, F. W. (1983) Complete nucleotide sequence of bacteriophage T7 and the locations of T7 genetic elements. *J. Mol. Biol. 166*, 477–535.

58. Li, H., Chelladurai, B. S., Zhang, K., and Nicholson, A. W. (1993) Ribonuclease III cleavage of a bacteriophage T7 processing signal. Divalent cation specificity, and specific anion effect. *Nucleic Acids Res. 21*, 1919–1925.
59. Chelladurai, B., Li, H., Zhang, K., and Nicholson, A. W. (1993) Mutational analysis of a ribonuclease III processing signal. *Biochemistry 32*, 7549–7558.
60. Dunn, J. J. (1976) RNase III cleavage of single-stranded RNA. Effect of ionic strength on the fidelity of cleavage. *J. Biol. Chem. 251*, 3807–3814.
61. Dunn, J. J. (1982) Ribonuclease III, in The Enzymes (Boyer, P., Ed.) Vol. 15, pp 485−499, Academic Press, New York.
62. Robertson, H. D., Webster, R. E., and Zinder, N. D. (1968) Purification and properties of ribonuclease III from *Escherichia coli*. *J. Biol. Chem. 243*, 82–91.
63. Sun, W., and Nicholson, A. W. (2001) Mechanism of action of *Escherichia coli* ribonuclease III. Stringent chemical requirement for the glutamic acid 117 side chain, and Mn^{2+} rescue of the Glu117Asp mutant. *Biochemistry 40*, 5102–5110.
64. Campbell, F. E., Cassano, A. G., Anderson, V. E., and Harris, M. E. (2002) Pre-steady-state and stopped-flow fluorescence analysis of *Escherichia coli* ribonuclease III: insights into mechanism and conformational changes associated with binding and catalysis. *J. Mol. Biol. 317*, 21–40.
65. Cambillau, C., and Claverie, J.-M. (2000) Structural and genomic correlates of hyperthermostability. *J. Biol. Chem. 275*, 32383–32386.
66. Suhre, K., and Claverie, J.-M. (2003) Genomic correlates of hyperthermostability, an update. *J. Biol. Chem. 278*, 17198–17202.
67. Calin-Jageman, I., and Nicholson, A. W. (2003) Mutational analysis of an RNA internal loop as a reactivity epitope for *Escherichia coli* ribonuclease III substrates. *Biochemistry 42*, 5025–5034.
68. Zhang, Y., Thiele, I., Weekes, D., Li, Z., Jaroszewski, L., Ginalksi, K., Deacon, A. M., Wooley, J., Lesley, J. A., Wilson, I. A., Palsson, B., Osterman, A., and Godzik, A. (2009) Three-dimensional structural view of the central metabolic network of *Thermotoga maritima*. *Science 325*, 1544–1549.